



The filter loading effect by ambient aerosols in filter absorption photometers depends on the mixing state of the sampled particles

5 Luka Drinovec^{1,2}, Asta Gregorič³, Peter Zotter^{4#}, Robert Wolf⁴, Emily Anne Bruns⁴, André S.H. Prévôt⁴, Jean-Eudes Petit^{5,6§}, Olivier Favez⁵, Jean Sciare^{6,7}, Ian J. Arnold^{8%}, Rajan K. Chakrabarty⁸⁺, Hans Moosmüller⁸, Agnes Filep⁹, Griša Močnik^{1,2}

[1] Research and Development Department, Aerosol d.o.o., Ljubljana, Slovenia

10 [2] Condensed Matter Physics Department, Jožef Stefan Institute, Ljubljana, Slovenia

[3] Center for Atmospheric Research, University of Nova Gorica, Nova Gorica, Slovenia

[4] Laboratory of Atmospheric Chemistry, Paul Scherrer Institute (PSI), 5232 Villigen PSI, Switzerland

[5] Institut National de l'Environnement Industriel et des Risques, Verneuil-en-Halatte, France

15 [6] Laboratoire des Sciences du Climat et de l'Environnement (CNRS-CEA-UVSQ), CEA Orme des Merisiers, Gif-sur-Yvette, France

[7] Energy Environment and Water Research Center, The Cyprus Institute, Nicosia, Cyprus

[8] Desert Research Institute, Nevada System of Higher Education, Reno, USA

[9] MTA-SZTE Research Group on Photoacoustic Spectroscopy, Department of Optics and Quantum Electronics, University of Szeged, Szeged, Hungary

20 [#] now at: Lucerne University of Applied Sciences and Arts, School of Engineering and Architecture, Bioenergy Research, Horw, Switzerland

[\$] now at: Air Lorraine, Metz, France

[+] now at: Department of Energy, Environmental & Chemical Engineering, Washington University in St. Louis, St. Louis, MO, USA

25 [%] now at: College of Optical Sciences, University of Arizona, Tucson, AZ, USA

Correspondence to: Luka Drinovec (luka.drinovec@aerosol.si) & Griša Močnik (grisa.mocnik@aerosol.si)



Abstract. Black carbon is a primary aerosol tracer for high-temperature combustion emissions and can be used to characterize the time evolution of its sources. It is correlated with a decrease in public health and contributes to atmospheric warming. Black carbon measurements are usually conducted with absorption filter photometers, which are prone to the filter-loading effect – a saturation of the instrumental response due to the accumulation of the sample in the filter matrix. In this paper, we investigate the hypothesis that this filter-loading effect depends on the optical properties of particles present in the filter matrix, especially on the black carbon particle mixing state. We conducted field campaigns in contrasting environments to determine the influence of source characteristics, particle age and coating on the magnitude of the filter-loading effect. High time resolution measurements of the filter-loading parameter in filter absorption photometers show daily and seasonal variations of the effect. The variation is most pronounced in the near-infrared region, where the black carbon mass concentration is determined. During winter, the filter-loading parameter value increases with the absorption Ångström exponent. It is suggested that this effect is related to the size of the black carbon particle core as the wood burning (with higher values of the absorption Ångström exponent) produces soot particles with larger diameters. A reduction of the filter-loading effect is correlated with the availability of the coating material. As the coating of ambient aerosols is reduced or removed, the filter-loading parameter increases. Coatings composed of ammonium sulfate and secondary organics seem to be responsible for the variation of the loading effect. The potential source contribution function analysis shows that high values of the filter-loading parameter in the infrared are indicative of local pollution, whereas low values of the filter-loading parameter result from ageing and coating during long range transport. Our results show that the filter-loading parameter can be used as proxy for determination of the particle mixing state, thus allowing for differentiation between local/fresh and transported/aged particles.

50

Keywords: black carbon, mixing state, Aethalometer, filter-loading effect



1 Introduction

55 Black carbon is a primary aerosol tracer for high-temperature combustion emissions and can be used to
characterize the time evolution of its sources (Lack et al., 2014). Investigations performed on ambient black
carbon mass equivalent concentrations (*BC*) have shown a stronger correlation with adverse public health effects
60 than the ones observed for the total mass of particulate matter (Janssen et al., 2011; Janssen et al., 2012;
Grahame et al., 2014; Olstrup et al., 2016). Black carbon absorbs sunlight very efficiently and heats the
atmosphere with the top of the atmosphere forcing exceeding 1 W/m^2 , and even though its lifetime is short
compared to CO_2 , it is still the second most important warming agent (Bond et al., 2013). Models show that its
short lifetime opens up the possibilities for short-term mitigation of atmospheric warming (Shindell et al., 2012).
While health effects are of interest in the context of local air pollution, climate change is investigated on regional
and global scales and co-benefits from black carbon emission reductions are of great interest (Smith et al., 2009).
65 Measurements are conducted at locations suitable for all three different scales, with absorption filter photometers
being the most common instrumentation employed to determine ambient black carbon mass concentrations.

Filter photometers measure the change of light transmitted by or reflected from the fiber filter on which particles
are collected. These methods feature high sensitivity and high time resolution. The measurements are, however,
70 prone to the filter-loading effect (FLE), a saturation of the instrumental response due to the accumulation of the
sample in the filter matrix (Bond et al., 1999; Weingartner et al., 2003; Moosmüller et al., 2009). This non-
linearity depends on the filter material and the type of instrument (Virkkula et al., 2007; Collaud Coen et al.,
2010; Hyvärinen et al., 2013). It is important to compensate for FLE to obtain accurate measurements of black
carbon concentration and for the determination of aerosol absorption spectra, which are used for source
75 apportionment (Kirchstetter et al., 2004; Sandradewi et al., 2008).

The filter loading effect, that is the reduction of the measurement sensitivity with increasing filter loading, in
Aethalometers has been described by several models (Weingartner et al., 2003; Arnott et al., 2005; Schmid et al.,
2006; Virkkula et al., 2007; Park et al., 2010; Collaud Coen et al., 2010; Drinovec et al., 2015). Offline methods
80 for the quantification of FLE are based on jumps of reported *BC* values just before and immediately after the
filter change (Weingartner et al., 2003; Virkkula et al., 2007) or *BC* vs. *ATN* method (Park et al., 2010; Segura et
al., 2014; Drinovec et al., 2015). These low time resolution estimations of FLE showed big differences in the
effect between seasons (Virkkula et al., 2007). Uncoated soot induces a higher loading effect compared to coated
soot (Weingartner et al., 2003) and Virkkula et al. (2015) showed that the loading parameter depends on the
85 backscatter fraction and the single scattering albedo (*SSA*).

Traditionally, Aethalometer data have been post-processed using fixed parameters characterizing the loading
effect. With the introduction of the dual-spot Aethalometer it has become possible to measure FLE with high
time resolution (Drinovec et al., 2015). This allows for a much better characterization of effects governing FLE.
90 In this paper, we are testing the hypothesis that the filter loading effect depends on the optical properties of
particles present in the filter matrix, especially on black carbon particle coating. Under laboratory conditions,
coating can enhance optical absorption of soot particles by up to factor of two (Weingartner et al., 2003;



Schnaiter et al., 2003). Ambient experiments show a smaller effect from 6%-60% (Cappa et al., 2012; Moffet and Prather, 2009; Liu et al., 2015). Determination of the mixing state using FLE may also reduce uncertainties
 95 in radiative forcing estimates (Jacobson, 2001; Shiraiwa et al., 2008). We conducted field campaigns in contrasted environments to determine the influence of sources, particle age and coating on the magnitude of the FLE.

2 Materials and Methods

100

2.1 Instrumentation

BC was characterized with the dual-spot Aethalometer (Magee Scientific Aethalometer model AE33) with real-time loading compensation (Drinovec et al., 2015). The inlet air stream of the AE33 is split and the sample is
 105 collected on two filter spots concurrently within the instrument. The flow through each of the two spots is different so that loading rates on the respective sample spots are different. Different loading rates cause the accumulation of the sample to be different between the two spots, resulting in the different magnitude of FLE between the spots. Measurement of FLE enables the compensation of the data – using the parametrization described in Drinovec et al. (2015), the compensation parameter *k* can be derived. This parameter describes the
 110 linear decrease of the instrumental sensitivity with loading of the spot with the absorbing sample for each wavelength of light at which the measurement is performed. The absorption coefficients are calculated at all wavelengths and *BC* is determined from the measurement at the wavelength 880 nm. Absorption and *BC* are compensated using the following equation:

$$115 \quad BC_{\text{compensated}}^{\lambda} = BC_{\text{non-compensated}}^{\lambda} / (1 - k_{\lambda} \cdot ATN_{\lambda}), \quad (1)$$

where *ATN* is optical attenuation of light passing through a sample loaded filter. $k_1, k_2, k_3, k_4, k_5, k_6, k_7$ are compensation parameters determined at the following wavelengths: 370, 470, 520, 590, 660, 880 and 950 nm. The absorption Ångström exponent (*AAE*) (Ångström, 1929) is calculated from absorption coefficient *b*
 120 (Drinovec et al., 2015) measured at 470 nm and 950 nm: $AAE = \ln(b_{470 \text{ nm}}/b_{950 \text{ nm}})/\ln(950/470)$. Instruments were run at 5 lpm sample flow and 1 minute time resolution.

The measurement of non-refractory submicron (NR-PM₁) major chemical species (i.e., organic matter, nitrate, sulphate, ammonium and chloride) was performed using Aerodyne® Aerosol Mass Spectrometer (AMS) and/or
 125 Aerosol Chemical Speciation Monitor (ACSM), fully described elsewhere (Canagaratna et al., 2007; Ng et al., 2011; Fröhlich et al., 2013). Briefly, PM_{2.5} aerosols are sampled at 3 L/min and then sub-sampled at about 85 mL/min through an aerodynamic lens, focusing submicron particles onto a 600°C-heated conical tungsten vaporizer where non-refractory material are flash-vaporized and quasi-instantaneously ionized by electron impact at 70 eV. AMS mainly differs from ACSM system by allowing for size-segregated measurements of the
 130 chemical composition by using a chopper in the AMS. Many AMS also use advanced mass spectrometers with higher resolution and better detection limits. However, for the measurements of NR-PM₁ species in ambient air,



a good agreement is commonly observed between data from these two instruments (Crenn et al., 2015; Fröhlich et al., 2015).

135 Individual aerosol particles were analyzed using field emission scanning electron microscope (FEG SEM, JEOL JSM 7100F TTLS) coupled with energy dispersive X-ray (EDX) system (X-Max Large Area Analytical Silicon Drift detector, Oxford Instrument). Aluminum foils used for sampling of aerosol particles (sampling described in section 2.2) were mounted directly on the sample holder by double-sided conductive carbon tape. SEM-EDX acquisitions were performed under high vacuum at 5 keV accelerating voltage. Micrographs were acquired by
140 secondary electron detector at 4 – 6 mm working distance (WD). Samples were first scanned under low magnification to obtain overall distribution of particles and afterwards closely examined at magnifications from 10,000 to 50,000. Representative areas were chosen for further EDX analyses. The microanalysis was performed at 10 mm WD with acquisition time of 50 to 150 s.

145 **2.2 Measurement campaigns**

The Paris campaigns were conducted at the SIRTAs observatory located about 20 km south of Paris, France (48° 42' 47" N, 2° 12' 29" E). The observatory sits on a plateau, about 160 m above sea level, in a semi-urban environment being divided between agricultural fields, wooded areas, housing and industrial developments. The
150 prevailing winds are from the South-West, blowing air of maritime origin over the site (e.g., Crippa et al., 2013). North-easterly winds also occur quite frequently under high pressure systems. The latter conditions are associated with the advection of continental air masses as well as of polluted air from the Paris metropolitan area. Beside continuous AE33 and ACSM measurements since 2013, results from two intensive EMEP campaigns in summer 2012 (15 June 2012 – 10 July) and winter 2013 (24 January 2013 – 16 February) were
155 available for the present study.

The Payerne station is a rural background air quality monitoring station located in Southwestern Switzerland (46° 48' 47" N, 6° 56' 40" E, 489 m a.s.l.), between the Jura and the Alps. It is situated about 1 km south-east of the small rural town of Payerne (Switzerland). The site is surrounded by agricultural land (grassland and crops),
160 forests, and small villages. Intensive campaigns took place in summer (15 June 2012 – 10 July 2012) and winter (24 January 2013 – 16 February 2013). In addition to the Aethalometer AE33, a high resolution ToF-AMS (Aerodyne Research) was operated throughout the campaigns.

The Ljubljana campaign was held between 6 August 2014 and 12 September 2014 in a suburban background
165 location, 10 km south-west of Ljubljana, Slovenia (46° 0' 58" N, 14° 24' 42" E), 293 a.s.l. The site is at the edge of a village surrounded by agricultural fields and at a distance of 500 m from a highway. It lies in the Ljubljana basin, which is surrounded by hills rising from 500 to 1700 m above the valley floor. The Ljubljana campaign used four AE33Aethalometers measuring four different ambient air streams: non-treated, dried, thermodenuded, and thermodenuded and dried samples. Ambient, dried and thermodenuded air streams had separate inlets; the
170 thermodenuded sample was separated in two streams, one connected directly to the Aethalometer, the second guided through a silica gel drier. The Dekati thermodenuder was set to a temperature of 300 °C with 10 l/min



sample flow, which was split for the two Aethalometers. The thermodenuder consists of a heated section and an air-cooled denuder where semi-volatile compounds are adsorbed onto activated charcoal. The estimated residence time for 10 l/min flow was 0.5 s. A diffusion membrane drier (Magee Scientific, Aerosol Inlet Dryer) and a silica gel drier with dew point reductions of 11.0 ± 1.0 °C and 11.5 ± 1.0 °C, respectively, were used. Scanning Mobility Particle sizer (SMPS) with a DMA (TSI, Model 3080) connected to a water-based Condensation Particle Counter (TSI, Model 3785 UWCPC) was used to acquire particle size distribution every 5 minutes. A Dekati DLPI low-pressure impactor was used to sample particles into 13 size fractions (from 30 nm to 10 µm) for scanning electron microscopy (SEM) and energy-dispersive X-ray (EDX) spectroscopy analysis. Impactor samples were collected on aluminum foils (DEKATI, CF-300) covered by a thin layer of APIEZON L grease. Impactor stage 4 with an expected particle size range between 170 – 260 nm was analyzed.

The K-pusztá campaign took place at K-pusztá observatory (Hungary, 46° 58' 12" N, 19° 33' E, 125 m a.s.l.) during January and February 2013. During winter ambient aerosols are dominated by wood burning emissions from household heating. The laboratory biomass burning profile was obtained during an experiment performed at the Paul Scherrer Institute (Bruns et al., 2015). Laboratory diesel exhaust was characterized at Aerosol d.o.o. in Ljubljana from a EURO 3 diesel engine. Exhaust was transferred into the smog chamber, where it was diluted and analyzed. Ljubljana roadside measurements were conducted during November 2012 in the city center, close to a heavy traffic road. Paris and Payerne data were collected during summer intensive campaigns (see above).

The Reno laboratory experiment was conducted at Desert Research Institute (Reno, Nevada, USA). Pure mustard oil was burned in a simple ceramic bowl with a cotton wick. The diluted emissions were collected and injected into a distribution chamber from which the sample was routed to multiple instruments. Ponderosa pine needles (~ 50 grams) were combusted in a biomass combustion chamber, a close replica of which has been described by Tian et al. (2015). The emissions from the first 35 seconds of combustion were collected in the distribution chamber and analyzed by a SMPS (TSI, DMA model 2080 with CPC model 3775) and an Aethalometer (model AE33).

2.3 Trajectory analysis

To illustrate air mass origin during specific pollution episodes during the Paris and Payerne campaigns (please see section 2.2), 72 h backtrajectories were calculated every 3 h using the PC-based version (v.4.9) of HYSPLIT (Stein et al., 2015) with weekly Global Data Assimilation System (GDAS) meteorological field data. Backtrajectories were set to end at SIRTÀ and Payerne at 500 m above ground level (a.g.l.).

Potential Contribution Source Function (PSCF), was used to investigate the potential advection of particulate material over large geographical scales during the different measurement campaigns. In this methodology, the probability that an air parcel may be responsible for high concentrations measured at the receptor site is calculated based on back-trajectory analyses, as described in Polissar et al. (1999). Briefly, at each *ij*-th grid cells, probabilities are calculated as:

210



$$PSCF_{ij} = \frac{m_{ij}}{n_{ij}} \quad , \quad (2)$$

where n_{ij} represents the total number of back-trajectories passing through each ij -th cell, and m_{ij} the number of back-trajectories passing through the same cell that are associated with measured concentrations higher than a user-defined threshold. A $0.5^\circ \times 0.5^\circ$ grid cell was used, covering Western Europe. Similarly to Waked et al. (2014), wet deposition was roughly estimated with precipitation data along each trajectory, assuming that even low precipitation would clean up the air parcel. For graphical purpose, results were smoothed by a Gaussian filter, and eventually normalized (see fig. 9 with colors scales from 0 to 1).

220 3. Results

3.1 Variability of filter loading effect (FLE)

The magnitude of the FLE for aerosols collected on a filter is dynamically determined by the dual-spot Aethalometer (Drinovec et al., 2015). The FLE depends on the entirety of the sample accumulated in the filter matrix up to the time of the measurement. The value of the FLE compensation parameter k is calculated for each of the seven measurement wavelengths, yielding a specific spectral fingerprint, which differs substantially between different measurement campaigns (Figure 1). The campaign-averaged values of the loading parameter k for short wavelengths show limited variability with a range of 0.004 – 0.005, while the variability in the near-infrared is much greater with a range of 0.001 – 0.008 (Table 1 and Figure 1).

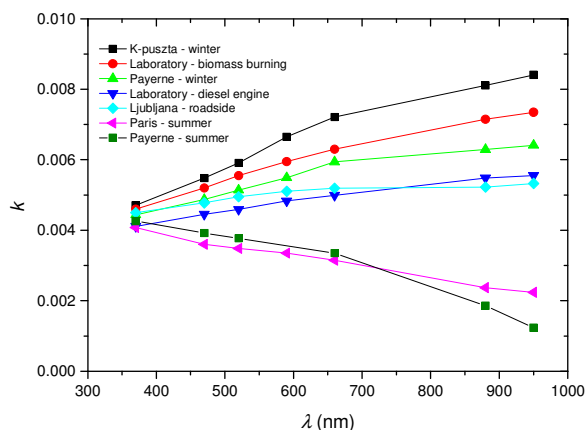


Figure 1: Typical spectral fingerprints of the FLE compensation parameter k obtained during ambient and laboratory campaigns. Campaign/experiment average values are presented.



235 **Table 1: Typical wavelength dependence of the filter loading compensation parameter k obtained for ambient and laboratory campaigns. Campaign average k and absorption Ångström exponent AAE are presented.**

		K-pusztza winter	Laboratory biomass burning	Payerne winter	Laboratory diesel engine exhaust	Ljubljana roadside	Paris summer	Payerne summer
AAE		1.55	1.40	1.35	1.04	0.97	1.06	1.16
Filter loading parameter k at the wavelength	370 nm	0.0047	0.0046	0.0044	0.0041	0.0045	0.0041	0.0043
	470 nm	0.0055	0.0052	0.0049	0.0045	0.0048	0.0036	0.0039
	520 nm	0.0059	0.0056	0.0051	0.0046	0.0050	0.0035	0.0038
	590 nm	0.0067	0.0060	0.0055	0.0048	0.0051	0.0034	NA
	660 nm	0.0072	0.0063	0.0059	0.0050	0.0052	0.0032	0.0034
	880 nm	0.0081	0.0072	0.0063	0.0055	0.0052	0.0024	0.0019
	950 nm	0.0084	0.0074	0.0064	0.0056	0.0053	0.0023	0.0012

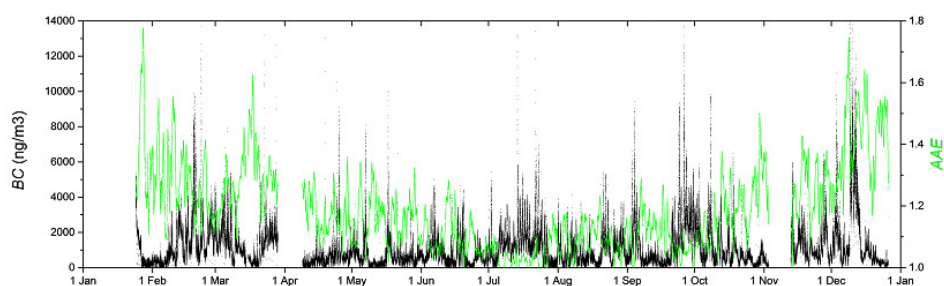
Table 1 also reports the average value of the absorption Ångström exponent obtained for each campaign. Occurrence of higher k values appears to be linked to the latter parameter, which is commonly used as a tracer for biomass burning aerosols (Kirchstetter et al., 2004; Sandradewi et al., 2008). This is evident for both laboratory and ambient data, the most extreme case for field campaigns being K-Pusztza winter data. For fresh diesel exhaust (laboratory and Ljubljana roadside measurements), obtained k values fall in the middle of the parameter range, whereas lower k values are obtained for summer ambient (Paris and Payerne) campaigns. This variability will be investigated in more detail in the following chapter.



3.2 Seasonal variation of filter loading effect

250 One-year-long black carbon mass concentrations at SIRTA show significant day-to-day variability with yearly average and standard deviation of $1068 \pm 1123 \text{ ng/m}^3$ (Figure 2). Average concentrations are of $913 \pm 932 \text{ ng/m}^3$ and $1263 \pm 1299 \text{ ng/m}^3$ respectively for the hot (April - September) and cold (October - March) periods, respectively. The sources of black carbon impacting the measurement site vary during the year; during summer the absorption Ångström exponent (AAE) is close to 1, indicating the dominance of traffic emissions, while

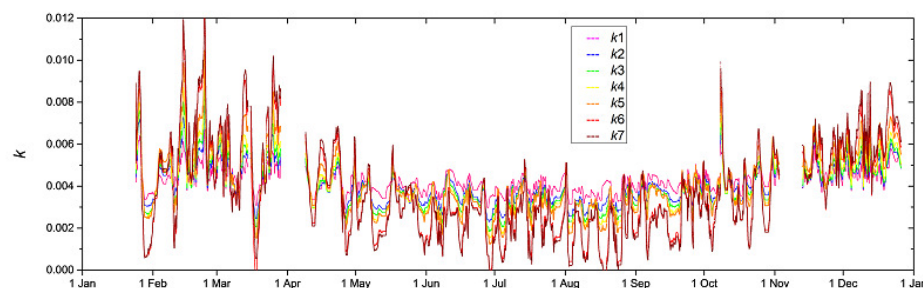
255 during winter its value is 1.4, suggesting the importance of biomass burning from residential heating (Kirchstetter et al., 2004; Sandradewi et al., 2008), which is consistent with previous BC source apportionment studies performed in the Paris area during intensive campaigns (e.g., Favez et al., 2009; Petit et al., 2014) as well as long-term investigations (Petit et al., 2015).



260 **Figure 2: Black carbon mass concentration and absorption Ångström exponent AAE measured at the Paris urban background site (SIRTA observatory) during 2013.**

Concomitantly with the absorption Ångström exponent, the parameter k shows large seasonal variations (Figure 3). Our investigation is focused here on k_6 ($\lambda = 880 \text{ nm}$), because of larger k variability at longer wavelengths

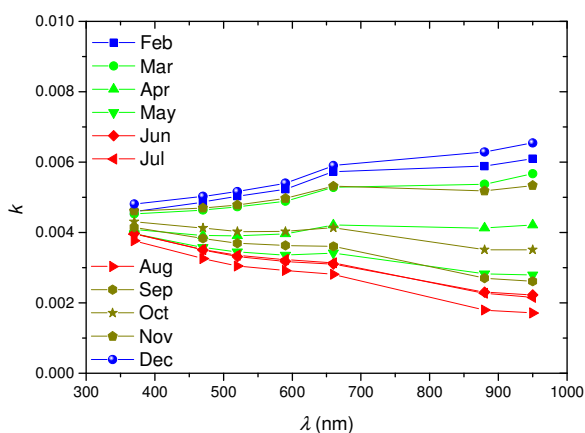
265 (Drinovec et al., 2015; Virkkula et al., 2015), and since Aethalometer measurements at 880 nm are traditionally used for the determination of black carbon mass concentrations. High values of k_6 , between 0.006 and 0.012 are observed during winter, while in summer k_6 remains low, with still large oscillations (0 – 0.005), with episodes of low k_6 that can last for several days, indicating stronger influence of weather conditions than of daily cycles.



270 **Figure 3: Filter loading parameter k measured at the Paris urban background site (SIRTA observatory) in 2013.**



Figure 4 shows monthly spectral fingerprints of the parameter k , which are in agreement with the offline analysis of the Aethalometer data (Virkkula et al., 2007; Virkkula et al., 2015): we measured the lowest values of the parameter k during summer (red) and highest during winter (blue) months, with spring and autumn somewhere in between. Again, the variation of the parameter k_6 roughly correlates to the AAE , except for the months of April, May, and October, when the k_6 monthly mean varies between 0.0028 and 0.0041, while the AAE mean changes very little between these months (Table 2). This seems to indicate that two distinct factors - meteorology and sources - may significantly influence the value of the parameter k .



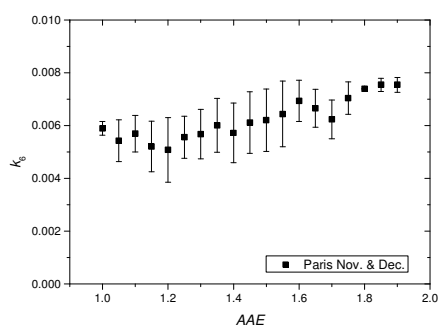
280 **Figure 4: Monthly spectral fingerprints of the filter loading effect compensation parameter k , obtained during the Paris campaign (SIRTA observatory) in 2013.**

285 **Table 2: Monthly averages and standard deviation of black carbon mass concentration BC , absorption Ångström exponent AAE and compensation parameter k_6 for the Paris campaign (SIRTA observatory) in 2013.**

Month	BC (ng/m^3)	AAE	k_6
February	1390 ± 1320	1.28 ± 0.47	0.0059 ± 0.0023
March	1370 ± 1070	1.29 ± 0.23	0.0054 ± 0.0024
April	570 ± 640	1.17 ± 0.43	0.0041 ± 0.0016
May	640 ± 660	1.16 ± 0.46	0.0028 ± 0.0011
June	750 ± 670	1.10 ± 0.37	0.0023 ± 0.0010
July	1250 ± 1000	1.04 ± 0.31	0.0023 ± 0.0010
August	870 ± 690	1.09 ± 0.32	0.0018 ± 0.0012
September	1310 ± 1380	1.10 ± 0.29	0.0027 ± 0.0010
October	960 ± 910	1.18 ± 0.33	0.0035 ± 0.0015
November	1180 ± 950	1.25 ± 0.25	0.0052 ± 0.0009
December	1580 ± 1930	1.41 ± 0.26	0.0063 ± 0.0010



To analyze the influence of black carbon sources, we investigated in more detail the dependence of k_6 on the AAE during the heating season. The November – December period was analyzed because of stable weather conditions. The results confirm that k_6 increases with the AAE (Figure 5), indicating higher values for biomass burning emissions compared to traffic emissions. This is in agreement with the laboratory biomass burning experiment, where high k_6 values were also obtained (Figure 1). Figure 5 shows a value for k_6 close to 0.0055 at an absorption Ångström exponent of 1, as expected for diesel exhaust from source and ambient measurements (Table 1). We hypothesize that higher values of k_6 for biomass burning compared to diesel exhaust are related to the difference in black carbon agglomerate size which is investigated in more detail in the following section. Indeed, diesel engine exhaust soot mobility diameter was reported in 30 – 100 nm range (Harris and Maricq, 2001; Keskinen and Rönkkö, 2010; Ning et al., 2013) in contrast to the 130 – 160 nm range for wood-stove emissions (Laborde et al., 2013) and 260 – 590 nm for wildfires (China et al., 2013). In special cases of large-scale sooty and turbulent fires with long flame residence time it is possible to obtain super-aggregates with geometric diameter larger than 1 μm (Chakrabarty et al., 2014).



300

Figure 5: The correlation between the FLE compensation parameter k_6 and the absorption Ångström exponent AAE for November and December 2013 in Paris (SIRTA observatory).

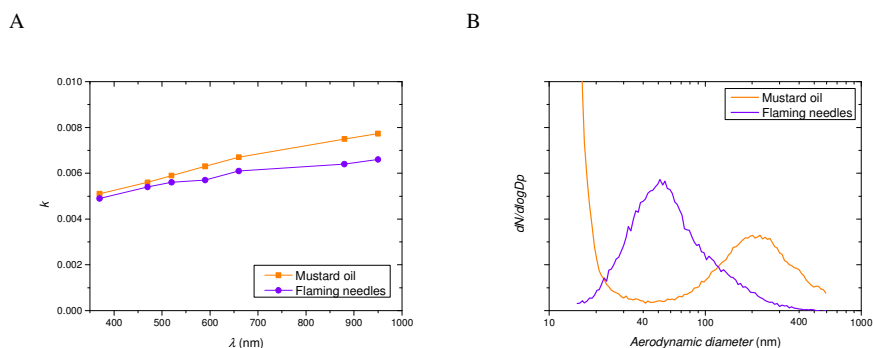


3.3 Particle size and the filter loading effect

305

To investigate the influence of black carbon particle size on k , we characterized emissions from a mustard oil lamp and from flaming ponderosa pine (*Pinus ponderosa*) needles combustion under laboratory conditions. Mustard oil burning produces particles with a mean mobility diameter of 210 nm (Figure 6A), which compares fairly well with the median aggregate mobility diameter of 296.8 ± 73.9 nm reported by Chakrabarty et al. (2013) for mustard oil lamp emissions. These particles are dominated by black carbon as indicated by an absorption Ångström exponent of 1 and low single scattering albedo of 0.23 (Table 3). Our Ångström exponent of 1 (470 nm, 950 nm) is somewhat lower than that determined by Chakrabarty et al. (2013, Fig. 2a) as 1.331 ± 0.004 (405 nm, 781 nm) with a three-wavelength photoacoustic instrument. Our single scattering albedo is in agreement with the lower values of 532-nm SSA measured by Chakrabarty et al. (2013, Fig. 4a) with an integrated photoacoustic-nephelometer. Chakrabarty et al. (2013) argue that higher values (up to ~ 0.8) of single scattering albedo shown in their Fig. 4 were caused by flickering of the flame increasing organic matter emissions; which may also have caused their increased absorption Ångström exponents. Flaming pine needle combustion produces considerably smaller particles with a mean diameter of 50 nm. We sampled only the flaming phase of Ponderosa pine needle combustion, where the emissions feature low values of the AAE (i.e., 1.25) and SSA (i.e., 0.49) as shown in Table 3. This is in agreement with the low SSA of 0.41 ± 0.14 at 532 nm that can be derived from the ratio of fuel-based emission factors of absorption and extinction cross sections measured by Chen et al. (2007, Table 1) with a photoacoustic absorption instrument and a CRD/CED extinction instrument, respectively, for flaming combustion of Ponderosa pine needles. We observed a larger filter loading effect for mustard oil lamp emissions (Figure 6a), which we believe is related to the larger particle size. This might explain the correlation between k and AAE in Figure 5. The values of the loading parameter for both sources and their wavelength dependence are similar to the ambient observations in winter (Figures 1 and 4). The loading parameter values for fresh combustion products seem to be influenced by the size of the combustion products with an approximately 15% increase in the IR wavelength region for an aerosol mobility diameter increase of about 4 times. The increase of the loading parameter in the IR with size is consistent with the reported soot particle diameters for different ambient sources (Ning et al., 2013; China et al., 2013). The difference in size is accompanied by the difference in the absorption Ångström exponent and single scattering albedo. In addition to the size dependence of k_0 , the dependence of the loading parameter on SSA we report here agrees with the one reported for Nanjing (Virkkula et al., 2015) – the decrease in SSA increases the loading parameter.

335



340 **Figure 6: The filter loading parameter k for laboratory measurements of emissions from mustard oil lamp and flaming Ponderosa pine needles (A). Aerosol size distributions for both sources (B).**

Table 3. Filter loading parameter k_6 , mean aerosol mobility diameter, single scattering albedo SSA at 532 nm and absorption Ångström exponent AAE of soot generated by mustard oil lamp and flaming Ponderosa pine needles.

	k_6	Particle size (nm)	$SSA_{532 \text{ nm}}$	AAE
Mustard oil lamp	0.0074 ± 0.0003	210	0.222 ± 0.003	1.02 ± 0.02
Flaming needles	0.0064 ± 0.0014	50	0.43 ± 0.05	1.25 ± 0.03

345



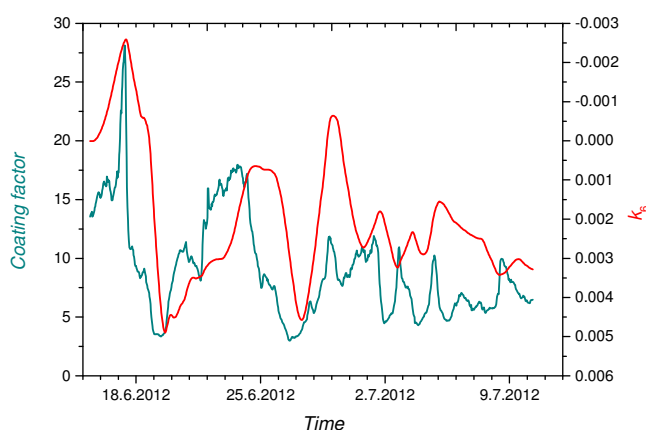
3.4 Influence of the mixing state on the filter loading effect: material available for coating

The second factor influencing k was assumed to be related to the meteorological conditions. To test this
350 assumption, high time resolution variation of k was investigated during EMEP campaigns taking place during
summer and winter in Paris and Payerne (Figure S1). During summer, we observed periods with k_6 close to zero,
which lasted for several days with short intervals with k_6 close to 0.005. During the winter campaigns, we
observed higher values of k_6 (up to 0.01) at both locations, whereas in Paris there were also two periods with low
 k_6 values. To investigate the dependence of the loading parameter k on the available coating material we
355 combined Aethalometer data with Payerne and Paris AMS/ACSM data. Here we define the coating factor (CF)
as a mass of the potential material available for coating (a sum of sulfate, ammonia, nitrate, and organic mass)
normalized to black carbon mass:

$$CF = (SO_4^{2-} + NO_3^- + NH_4^+ + ORG)/BC. \quad (3)$$

360

The time trend of CF and k_6 from the Paris summer campaign shows a similar time variation pattern (Figure 7).
High CF coincides with low value of parameter k_6 and vice versa. However, there is a time lag between both
measurements which is related to the way the loading parameter k is determined (Drinovc et al., 2015): the
parameter k is a cumulative property of all particles on the filter; hence all particles on the filter, collected from
365 the last time the tape has been advanced, contribute to the loading effect. This means that the time-lag varies
with and depends on ambient black carbon concentration. The second reason is geometric smoothing employed
in the algorithm, which takes the last k value determined from the previous filter spot into account. The time lag
impairs the k_6 vs CF correlation resulting in higher standard deviation of k_6 averaged in each CF bin (Figure 8).



370 **Figure 7: Coating factor and filter loading parameter k_6 time series during the Paris summer campaign. Note the inverted scale for k_6 .**

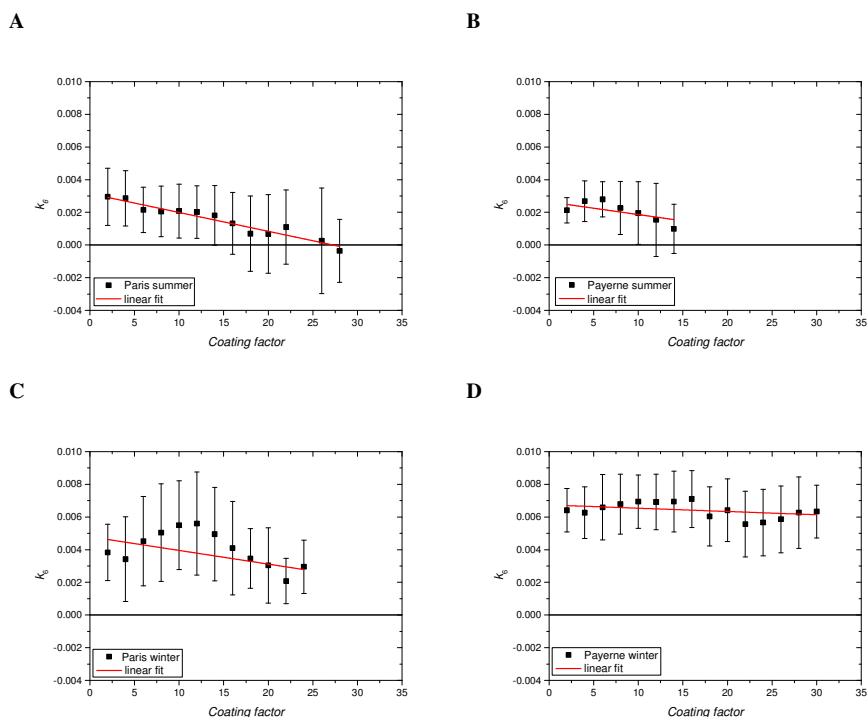


Figure 8: Correlation between the filter loading parameter k_6 and the coating factor CF during winter and summer campaigns in Paris and Payerne. Hourly data is averaged in CF bins 2 units wide. The error bars represent standard deviation for data points inside each bin.

Table 4: Fitting parameters of the filter loading parameter k_6 versus the coating factor and absorption Ångström exponent AAE during winter and summer campaigns in Paris and Payerne.

	slope (10^{-4})	intercept at $k_6=0$	AAE
Paris summer	-1.2 ± 0.1	27 ± 3	1.06
Payerne summer	-0.8 ± 0.5	35 ± 20	1.16
Paris winter	-0.8 ± 0.3	57 ± 22	1.34
Payerne winter	-0.2 ± 0.1	340 ± 180	1.35

We have observed a decrease of k_6 with increasing coating factor for all four campaigns. The results are most pronounced for the Paris summer campaign with the largest absolute slope of the linear regression line. In Payerne, the slope is slightly lower. In summer, k_6 reaches zero at coating factor values of approximately 30 for both locations (Table 4). These results show that during summer the coating material causes a reduction of the filter loading effect. In Paris, CF is much larger compared to Payerne. Because most of the non-refractory material in Paris during the summer is of secondary origin (Freutel et al. 2013), it is possible to form internally mixed aerosols in the atmosphere. The correlation of particle size with coating factor in Paris supports this assertion (Figure S2).



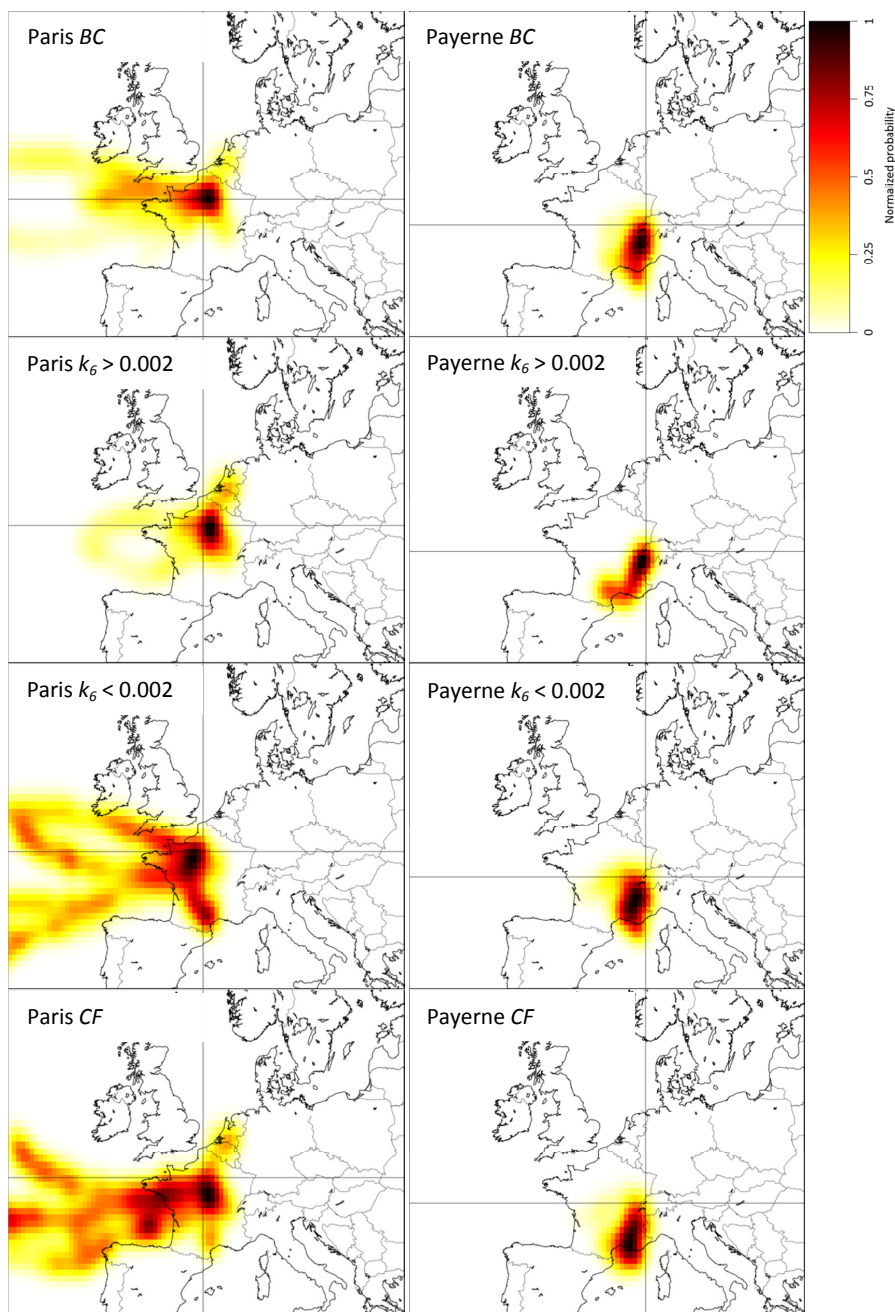
The slope obtained for the Paris winter campaign is lower compared to summer and k_6 reaches zero at $CF=57$, with the dependence being more complicated than the linear one observed in summer. There is almost no correlation between k_6 and CF during winter in Payerne. This might be a consequence of biomass burning emissions which are dominated by organics usually externally mixed with black carbon – as confirmed for Paris region during the MEGAPOLI campaign (Healy et al., 2013). The amount of black carbon and organics from biomass burning depends strongly on the combustion conditions, with black carbon being created at high temperature flaming combustion and organics at low temperature smoldering combustion (Chakrabarty et al., 2013; Pagels et al., 2013). Especially during summer, elevated amounts of secondary non-refractory material are available for coating and we observe a good correlation of k_6 with CF , which indicates that coating is responsible for reduction of filter loading effect. The decrease of k_6 with increasing CF is at first counterintuitive if it is compared with the influence of the measured aerosol mobility diameter on k_6 . It was observed that the increase in the mobility diameter may induce a k_6 increase (Figure 6), and one could speculate that the availability of material for coating black carbon cores, and hence a high value of CF , would increase the aerosol size and thereby increase the k_6 value. In fact, the contrary happens, increasing CF decreases k_6 . However, increase in CF should increase SSA as well, and it has been shown for ambient aerosols in Nanjing (Virkkula et al., 2015) that the increase in SSA decreases k_6 . To resolve this question in the following sections, we will investigate first the influence of aerosol age, and continue with removing or reducing aerosol coating.



3.5 Aerosol age and origin influence the filter loading effect

Influence of the aerosol age was indirectly investigated by using potential source contribution function (PSCF).
415 We divided the dataset into two subsets distinguished by k_6 being bigger or smaller than the campaign average of 0.002. The analysis was carried out for the summer period, when the planetary boundary layer is thicker compared to the winter with stronger influence of long-range transport than in winter, and good vertical mixing to the ground, where the measurement station is positioned.

420 In Paris, the compensation parameter k is very well correlated with aerosol age: high values indicate local sources while values close to zero indicate a regional contribution (Figure 9). For low k values it seems that the sources are distributed over France, part of Great Britain, and the Atlantic Ocean. This fact may be explained by influx of potential coating material that is brought to Paris by mid- and long-range transport and mixed with more local sources of black carbon (Bressi et al., 2013; Petit et al., 2015). In Payerne, the meteorological
425 situation is different having a smaller source area. This can be explained by the station being located between the Jura mountains and the Alps where the air is in general more stagnant compared to Paris, and is channeled from southwest to east-northwest due to the mountain ranges. Still we can observe that low k measurements are related to distributed sources further from the station. At both locations, the distribution of the coating factor resembles that of the low k_6 . This is in agreement with the correlation analysis in the chapter above, where k_6
430 decreases with CF (Figure 8, A, B). A low value of k_6 is indicative of aged particles, and a high value of fresh, local aerosols. This is in agreement with the spectral fingerprint of fresh diesel engine emissions (Figure 1). Measurements in Paris during the MEGAPOLI campaign showed that fresh traffic BC particles are non-coated, whereas BC particles from long-range transport exhibit substantial coatings of non-refractory material (Laborde et al., 2013). On average, regional transport contained 7 % of EC mass compared to 37 % from local emissions
435 (Healy et al., 2013), in accordance with our PSCF analysis of the coating factor. Theoretical studies show that coating consisting of secondary organic and inorganic species is mostly transparent in the visible part of the spectrum and can affect the absorption of light by the particles (Fuller et al., 1999; Bond et al., 2006). The fact that coating can increase absorption was confirmed in ambient studies (Wei et al., 2013b; Liu et al., 2015) and the coating may also be responsible for the decrease of parameter k .
440



445

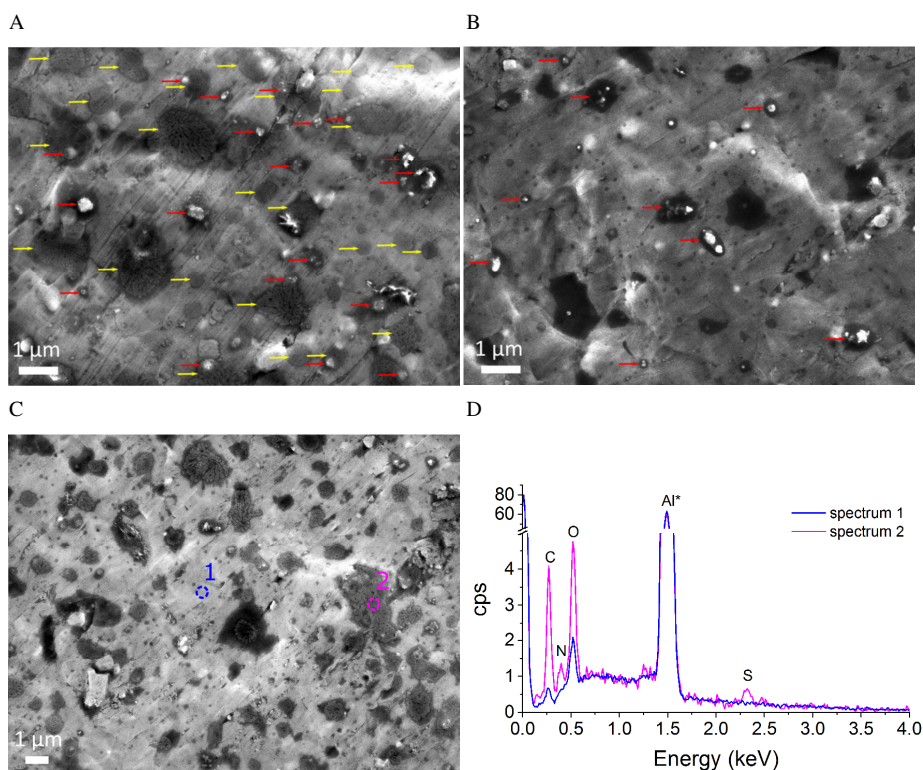
Figure 9: The potential source contribution function analysis in Paris and Payerne for measurement with low/high values of the filter loading compensation parameter k_6 , for the coating factor (CF) and black carbon (BC) being higher than 75th percentile.



450 **3.6 Influence of the mixing state on the filter loading effect: removing the coating of ambient aerosols**

Our coating hypothesis was put to the definite test during the Ljubljana campaign; we investigated the effect of the ambient aerosol coating thickness reduction on the loading effect. The campaign was carried out in summer, when the atmospheric mixing is stronger, so we expected aged and internally mixed aerosols to be ubiquitous.

455 We have used two approaches to reduce the coating thickness: drying and thermo-denuding the inlet stream. Drying is expected to influence particles coated with hygroscopic material; thermo-denuding was used to remove certain organic compounds (Huffman et al., 2009; Cappa et al., 2012; Liu et al., 2015), but it also removes nitrates and sulfates which decompose above 280° C (CRC, 1920). The thermo-denuder in our experiment was set to an operation temperature of 300° C. At this temperature part of low volatility oxygenated organic aerosols
460 (LV-OOA) is not removed from the sample (Poulain et al., 2014).



465

Figure 10: SEM images of ambient (A) and thermo-denuded (B) impactor samples (size range 170 – 260 nm) taken during the Ljubljana campaign. The energy-dispersive X-ray spectra (D) were obtained at the selected areas on image (C). Red and yellow arrows mark soot agglomerates and secondary ammonium sulfate residue, respectively.

470



The de-coating efficiency of the thermo-denuder was tested using SEM analysis of the impactor samples taken during mid-day, the time when a well-mixed atmosphere is expected. Coating residues were most pronounced for above-average size particles (Figure S4); thus the impactor stage with 170 – 260 nm particle size range was selected for the analysis (Figure 10). We can observe soot agglomerates (white, red arrows), organic residue (dark patches around agglomerates), and brain-shaped dendritic residues (yellow arrows). Dark patches around soot agglomerates can be also be found on the thermo-denuded sample, indicating low volatility of these compounds. The main difference between the non-perturbed and thermo-denuded sample is the removal of the dendrite-shaped residue; similarly shaped residue was reported in different studies (Buseck and Posfai, 1999; Adachi et al., 2014) as secondary ammonium sulfate particles. To confirm the presence of secondary inorganic particles and analyze their chemical composition, we utilized energy-dispersive X-ray spectroscopy (EDX). In the background area (Figure 10 C, spectrum 1), we identified spectral peaks specific for carbon, oxygen, and aluminum, as expected for impactor aluminum foil covered with thin layer of grease. In the residue area (spectrum 2) we observed carbon and oxygen peaks with higher amplitude compared to background, and additional sulfur and nitrogen peaks. This indicates the presence of oxidized organic compounds, ammonium sulfate, and possibly nitrates, further confirming the presence of coatings and in line with findings of previous studies (Adachi et al., 2014).



490 The de-coating experiment consisted of four instruments sampling ambient, dried, thermo-denuded, and thermo-
denuded and dried air streams simultaneously. Diurnal profiles of k_6 show qualitative and quantitative
differences between the four treatments (Figure 11): the loading parameter k_6 for ambient aerosols reaches its
highest value during the night and decreases during the afternoon, when the atmosphere is completely mixed.
Drying increases the average value of parameter k_6 and amplifies the night/day variation. For the thermo-
denuded samples, k_6 is almost constant during the day with higher average values for the thermo-denuded and
495 dried sample stream. The average campaign value of parameter k_6 shows a statistically significant difference
between all treatments ($p = 0.05$). The k_6 for thermo-denuded samples is similar to that of fresh diesel exhaust
(Table 1) as expected for ambient aerosol after removal of inorganic coating by the thermo-denuder. These
results are consistent with the findings of the coating factor analysis above, where coating causes reduction of k_6 .

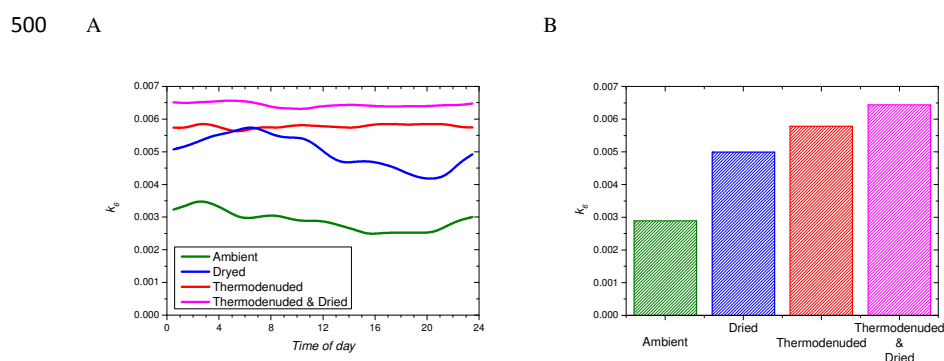


Figure 11: Influence of dried and/or thermo-denuded ambient aerosols on the filter loading parameter k_6 : diurnal plot (A) and campaign averages (B). Average values of k_6 for different treatments are significantly different with $p = 0.05$.

505 Freshly emitted BC particles are hydrophobic (Weingartner et al., 1997; Zuberi et al., 2005) and show low
relative humidity induced particle growth (Laborde et al., 2013). Immediately after sunrise, soot particles in the
atmosphere begin to age by developing a coating of secondary species including ammonium nitrate, sulfate, and
organics (Moffet and Prather, 2009). This coating makes particles hydrophilic and sensitive to relative humidity
510 induced growth (Hu et al., 2010; Zhang et al., 2015), which influences scattering and absorption (Wei et al.,
2013a; Wei et al., 2013b). Drying the inlet stream during the Ljubljana campaign reduced the thickness of the
hydrophilic coating and caused a large increase of k_6 . An even greater effect was observed for the thermo-
denuded sample, where most of the inorganic coatings were removed. Interestingly, we observed the effect of
drying also for thermo-denuded particles. This is attributed to the presence of oxygenated organic aerosols that
515 are less efficiently removed because of their low volatility (Huffman et al., 2009; Cappa and Jimenez, 2010;
Poulain et al., 2014). For the urban environment, it was shown that most of secondary (oxygenated) organic
aerosols are water-soluble (Kondo et al., 2007) and could be prone to relative humidity induced growth. This
experiment further supports the hypothesis that coating is responsible for the reduction of the filter loading effect
in Aethalometer.

520



4 Conclusions

We have tested the hypothesis that the filter loading effect present in filter-based photometers used for BC determination depends on the optical properties of particles present in the filter matrix, especially on coatings of black carbon particles. High time resolution measurements of the filter loading parameter in Aethalometer show daily and seasonal variations on the effect, which is most pronounced in the infrared region used for the determination of black carbon mass concentrations. The filter loading parameter value increases with the absorption Ångström exponent. It is suggested that this effect is related to the size of the black carbon agglomerates. The loading parameter for fresh combustion products seems to be influenced by the size of the combustion particles with an approximately 15% increase in the infrared wavelength region for an aerosol mobility diameter increase of about 4 times. On the other hand, we observed a reduction of the filter loading effect correlated with the availability of the coating material. High coating factor coincides with low value of loading parameter and vice versa. These results show that during summer the coating material causes reduction of filter loading effect. There is less or no correlation in winter, which may be a consequence of biomass burning organics being externally mixed with black carbon. To further test the coating hypothesis, a de-coating experiment using an aerosol drier and thermo-denuder was performed. De-coating the ambient aerosols increases the filter loading effect, as the coating is reduced or removed. The coating composed of ammonium sulfate and secondary organics seems to be responsible for the variation of the loading effect. The potential source contribution function analysis shows that high values of the filter loading parameter in the infrared are indicative of local pollution, whereas low values of the filter loading parameter result from ageing and coating during long range transport. Our results show that the filter loading parameter can be used as a proxy for determination of the particle mixing state, thus allowing to differentiate between local/fresh and transported/aged particles. Filter loading parameter is thus not only important for compensation of the Aethalometer absorption data but also provides additional information on the physical properties of aerosols.



Acknowledgements

The work described herein was supported by:

- EUROSTARS grant E!4825 FC Aeth
- 550 - JR-KROP grant 3211-11-000519
- JR-RK grant 3330-14-509063
- ACTRIS EU-FP7 grant n°262254
- 'PREQUALIF' project (ADEME contract n°1132C0020), DIM R2DS (AAP 2010)
- 'PARTICUL'AIR' project, and institutions CNRS, CEA and FEON.
- 555 - the National Science Foundation under Cooperative Support Agreement No. EPS-0814372
- NASA EPSCoR under Cooperative Agreement No. NNX14AN24A
- NASA ROSES under Grant No. NNX15AI48G
- National Science Foundation (NSF) under Grant No. AGS-1544425
- We thank the Slovenian Environmental Agency and AMES d.o.o. for the use of their measurement sites.
- 560

Conflict of interest declaration

- L. Drinovec and G. Močnik are employed by the company Aerosol d.o.o. which develops and manufactures aerosol instrumentation including the Aethalometer AE33 and the drier used in the campaigns. H. Moosmüller is
- 565 a co-inventor of the photoacoustic instruments (PASS and PAX) manufactured by Droplet Measurement Technologies and receives licensing fees from their sale.

570 **References**

- Adachi, K., Zaizen, Y., Kajino, M., and Igarashi, Y.: Mixing state of regionally transported soot particles and the coating effect on their size and shape at a mountain site in Japan, *J. Geophys. Res. Atmos.*, 119, 5386–5396, doi:10.1002/2013JD020880, 2014.
- 575 Ångström, A.: On the atmospheric transmission of sun radiation and on dust in the air, *Geogr. Ann.*, 11, 156–166, doi:10.2307/519399, 1929.
- Arnott, W. P., Hamasha, K., Moosmüller, H., Sheridan P. J., and Ogren, J. A.: Towards aerosol light-absorption measurements with a 7-wavelength aethalometer: evaluation with a photoacoustic instrument and 3-wavelength nephelometer, *Aeros. Sci. Tech.* 39(1): 17–29, doi:10.1080/027868290901972, 2005.
- 580 Bruns, E. A., Krapf, M., Orasche, J., Huang, Y., Zimmermann, R., Drinovec, L., Močnik, G., El-Haddad, I., Slowik, J. G., Dommen, J., Baltensperger, U., and Prévôt, A. S. H.: Characterization of primary and secondary wood combustion products generated under different burner loads, *Atmos. Chem. Phys.*, 15, 2825–2841, doi:10.5194/acp-15-2825-2015, 2015.
- Bond, T. C., Anderson, T. L., and Campbell, D.: Calibration and intercomparison of filter-based measurements of visible light absorption by aerosols, *Aerosol Sci. Tech.*, 30, 582–600, doi:10.1080/027868299304435, 1999.
- Bond, T. C., Habib, G., and Bergstrom, R. W.: Limitations in the enhancement of visible light absorption due to mixing state, *J. Geophys. Res.*, 111, D20211, doi:10.1029/2006JD007315, 2006.
- Bond, T. C., Doherty, S. J., Fahey, D. W., Forster, P. M., Berntsen, T., DeAngelo, B. J., Flanner, M. G., Ghan, S., Kärcher, B., Koch, D., Kinne, S., Kondo, Y., Quinn, P. K., Sarofim, M. C., Schultz, M. G., Schulz, M., Venkataraman, C., Zhang, H., Zhang, S., Bellouin, N., Guttikunda, S. K., Hopke, P. K., Jacobson, M. Z., Kaiser, J. W., Klimont, Z., Lohmann, U., Schwarz, J. P., Shindell, D., Storelvmo, T., Warren, S. G., and Zender, C. S.: Bounding the role of black carbon in the climate system: a scientific assessment, *J. Geophys. Res. Atmos.*, 118, 5380–5552, doi:10.1002/jgrd.50171, 2013.
- 590 Bressi, M., Sciare, J., Gherzi, V., Bonnaire, N., Nicolas, J. B., Petit, J.-E., Moukhtar, S., Rosso, A., Mihalopoulos, N., and Féron, A.: A one-year comprehensive chemical characterisation of fine aerosol (PM_{2.5}) at urban, suburban and rural background sites in the region of Paris (France), *Atmos. Chem. Phys.*, 13, 7825–7844, doi:10.5194/acp-13-7825-2013, 2013.
- Buseck P. R. and Posfai M.: Airborne minerals and related aerosol particles: Effects on climate and the environment, *Proc. Natl. Acad. Sci. USA.*, 96, 3372–3379, doi:10.1073/pnas.96.7.3372, 1999.
- 600 Canagaratna, M. R., Jayne, J. T., Jimenez, J. L., Allan, J. D., Alfarra, M. R., Zhang, Q., Onasch, T. B., Drewnick, F., Coe, H., Middlebrook, A., Delia, A., Williams, L. R., Trimborn, A. M., Northway, M. J., DeCarlo, P. F., Kolb, C. E., Davidovits, P., and Worsnop, D. R.: Chemical and microphysical characterization of ambient aerosols with the aerodyne aerosol mass spectrometer, *Mass Spectrom. Rev.*, 26(2), 185–222, doi:10.1002/mas.20115, 2007.
- 605 Cappa C. D. and Jimenez J. L.: Quantitative estimates of the volatility of ambient organic aerosol, *Atmos. Chem. Phys.*, 10(12), 5409–5424, doi:10.5194/acp-10-5409-2010, 2010.



- 610 Cappa, C. D. and Wilson, K. R.: Multi-generation gas-phase oxidation, equilibrium partitioning, and the formation and evolution of secondary organic aerosol, *Atmos. Chem. Phys.*, 12, 9505–9528, doi:10.5194/acp-12, 2012.
- Chakrabarty, R. K., Arnold, I. J., Francisco, D. M., Hatchett, B., Hosseinpour, F., Loria, M., Pokharel, A., and Woody, B. M.: Black and brown carbon fractal aggregates from combustion of two fuels widely used in Asian rituals, *J. Quant. Spectrosc. Ra.*, 122, 25–30, doi:10.1016/j.jqsrt.2012.12.011, 2013.
- 615 Chakrabarty, R. K., Beres, N. D., Moosmüller, H., China, S., Mazzoleni, C., Dubey, M. K., Liu, L., and Mishchenko, M. I.: Soot superaggregates from flaming wildfires and their direct radiative forcing, *Nat. Sci. Rep.*, 4, 5508, doi:10.1038/srep05508, 2014.
- Chen, L.-W. A., Moosmüller, H., Arnott, W. P., Chow, J. C., Watson, J. G., Susott, R. A., Babbitt, R. E., Wold, C. E., Lincoln, E. N., and Hao, W. M.: Emissions from laboratory combustion of wildland fuels: emission factors and source profiles, *Environ. Sci. Tech.*, 41(12), 4317–4325, doi: 10.1021/es062364i, 2007.
- 620 China S., Mazzoleni C., Gorkowski K., Allison C. A., and Dubey, M. K.: Morphology and mixing state of individual freshly emitted wildfire carbonaceous particles, *Nat. Comm.*, 4, 2122, doi:10.1038/ncomms3122, 2013.
- Crenn, V., Sciare, J., Croteau, P. L., Verlhac, S., Fröhlich, R., Belis, C. A., Aas, W., Äijälä, M., Alastuey, A., Artiñano, B., Baisnée, D., Bonnaire, N., Bressi, M., Canagaratna, M., Canonaco, F., Carbone, C., Cavalli, F., 625 Coz, E., Cubison, M. J., Esser-Gietl, J. K., Green, D. C., Gros, V., Heikkinen, L., Herrmann, H., Lunder, C., Minguillón, M. C., Močnik, G., O'Dowd, C. D., Ovadnevaite, J., Petit, J.-E., Petralia, E., Poulain, L., Priestman, M., Riffault, V., Ripoll, A., Sarda-Estève, R., Slowik, J. G., Setyan, A., Wiedensohler, A., Baltensperger, U., Prévôt, A. S. H., Jayne, J. T., and Favez, O.: ACTRIS ACSM intercomparison – Part 1: Reproducibility of concentration and fragment results from 13 individual Quadrupole Aerosol Chemical 630 Speciation Monitors (Q-ACSM) and consistency with co-located instruments, *Atmos. Meas. Tech.*, 8, 5063–5087, doi:10.5194/amt-8-5063-2015, 2015.
- Collaud Coen, M., Weingartner, E., Apituley, A., Ceburnis, D., Fierz-Schmidhauser, R., Flentje, H., Henzing, J. S., Jennings, S. G., Moerman, M., Petzold, A., Schmid, O., and Baltensperger, U.: Minimizing light absorption measurement artifacts of the Aethalometer: evaluation of five correction algorithms, *Atmos. 635 Meas. Tech.*, 3, 457–474, doi:10.5194/amt-3-457-2010, 2010.
- CRC (1920). *Handbook of Chemistry and Physics*, CRC Press, 8th edition.
- Crippa, M., I. El Haddad, J. G. Slowik, P. F. DeCarlo, C. Mohr, M. F. Heringa, R. Chirico, N. Marchand, J. Sciare, U. Baltensperger, and A. S. H. Prevot: Identification of marine and continental aerosol sources in Paris using high resolution aerosol mass spectrometry, *Journal of Geophysical Research-Atmospheres*, 640 118(4), 1950–1963, doi: 10.1002/jgrd.50151, 2013.
- Drinovec, L., Močnik, G., Zotter, P., Prévôt, A. S. H., Ruckstuhl, C., Coz, E., Rupakheti, M., Sciare, J., Müller, T., Wiedensohler, A., and Hansen, A. D. A.: The "dual-spot" Aethalometer: an improved measurement of aerosol black carbon with real-time loading compensation, *Atmos. Meas. Tech.*, 8, 1965–1979, doi:10.5194/amt-8-1965-2015, 2015.



- 645 Favez, O., Cachier, H., Sciare, J., Sarda-Estève, R., and Martinon, L.: Evidence for a significant contribution of wood burning aerosols to PM_{2.5} during the winter season in Paris, France, *Atmos. Environ.*, 43, 3640–3644, doi:10.1016/j.atmosenv.2009.04.035, 2009.
- Freutel, F., Schneider, J., Drewnick, F., von der Weiden-Reinmüller, S.-L., Crippa, M., Prévôt, A. S. H., Baltensperger, U., Poulain, L., Wiedensohler, A., Sciare, J., Sarda-Estève, R., Burkhardt, J. F., Eckhardt, S., 650 Stohl, A., Gros, V., Colomb, A., Michoud, V., Doussin, J. F., Borbon, A., Haeffelin, M., Morille, Y., Beekmann, M., and Borrmann, S.: Aerosol particle measurements at three stationary sites in the megacity of Paris during summer 2009: meteorology and air mass origin dominate aerosol particle composition and size distribution, *Atmos. Chem. Phys.*, 13, 933–959, doi:10.5194/acp-13-933-2013, 2013.
- Fröhlich, R., Cubison, M. J., Slowik, J. G., Bukowiecki, N., Prévôt, A. S. H., Baltensperger, U., Schneider, J., 655 Kimmel, J. R., Gonin, M., Rohner, U., Worsnop, D. R., and Jayne, J. T.: The ToF-ACSM: a portable aerosol chemical speciation monitor with TOFMS detection, *Atmos. Meas. Tech. Discuss.*, 6, 6767–6814, doi:10.5194/amt-d-6-6767-2013, 2013.
- Fröhlich, R., Crenn, V., Setyan, A., Belis, C. A., Canonaco, F., Favez, O., Riffault, V., Slowik, J. G., Aas, W., Aijala, M., Alastuey, A., Artinano, B., Bonnaire, N., Bozzetti, C., Bressi, M., Carbone, C., Coz, E., Croteau, 660 P. L., Cubison, M. J., Esser-Gietl, J. K., Green, D. C., Gros, V., Heikkinen, L., Herrmann, H., Jayne, J. T., Lunder, C. R., Minguillon, M. C., Mocnik, G., O'Dowd, C. D., Ovadnevaite, J., Petralia, E., Poulain, L., Priestman, M., Ripoll, A., Sarda-Estève, R., Wiedensohler, A., Baltensperger, U., Sciare, J., and Prevot, A. S. H.: ACTRIS ACSM intercomparison - Part 2: Intercomparison of ME-2 organic source apportionment results from 15 individual, co-located aerosol mass spectrometers, *Atmospheric Measurement Techniques*, 665 8(6), 2555–2576, doi:10.5194/amt-8-2555-2015, 2015.
- Fuller, K. A., Malm, W. C., and Kreidenweis, S. M.: Effects of mixing on extinction by carbonaceous particles, *J. Geophys. Res.*, 104:15, 941–915, doi:10.1029/1998JD100069, 1999.
- Grahame, T. J., Klemm, R., and Schlesinger, R. B.: Public health and components of particulate matter: The changing assessment of black carbon, *J. Air Waste Manage.*, 64, 620–660, 670 doi:10.1080/10962247.2014.912692, 2014.
- Harris S. J. and Maricq M. M.: Signature size distributions for diesel and gasoline engine exhaust particulate matter, *Aeros. Sci.*, 32, 749–764. doi:10.1016/S0021-8502(00)00111-7, 2001.
- Healy, R. M., Sciare, J., Poulain, L., Crippa, M., Wiedensohler, A., Prévôt, A. S. H., Baltensperger, U., Sarda- 675 Estève, R., McGuire, M. L., Jeong, C.-H., McGillicuddy, E., O'Connor, I. P., Sodeau, J. R., Evans, G. J., and Wenger, J. C.: Quantitative determination of carbonaceous particle mixing state in Paris using single-particle mass spectrometer and aerosol mass spectrometer measurements, *Atmos. Chem. Phys.*, 13, 9479–9496, doi:10.5194/acp-13-9479-2013, 2013.
- Hu, D., Qiao, L., Chen, J., Ye, X., Yang, X., Cheng, T., and Fang, W.: Hygroscopicity of inorganic aerosols: Size and relative humidity effects on the growth factor, *Aerosol. Air. Qual. Res.*, 10, 255–264, 680 doi:10.4209/aaqr.2009.12.0076, 2010.
- Huffman, J. A., Docherty, K. S., Aiken, A.C., Cubison, M. J., Ulbrich, I. M., DeCarlo, P. F., Sueper, D., Jayne, J. T., Worsnop, D. R., Zieann, P. J., and Jimenez, J. L.: Chemically-resolved aerosol volatility measurements from two megacity field studies, *Atmos. Chem. Phys.*, 9, 7161–7182, doi:10.5194/acp-9-7161-2009, 2009.



- 685 Hyvärinen, A.-P., Vakkari, V., Laakso, L., Hooda, R. K., Sharma, V. P., Panwar, T. S., Beukes, J. P., van Zyl, P. G., Josipovic, M., Garland, R. M., Andreae, M. O., Pöschl, U., and Petzold, A.: Correction for a measurement artifact of the Multi-Angle Absorption Photometer (MAAP) at high black carbon mass concentration levels, *Atmos. Meas. Tech.*, 6, 81-90, doi:10.5194/amt-6-81-2013, 2013.
- Jacobson, M. Z.: Strong radiative heating due to the mixing state of black carbon in atmospheric aerosols, *Nature*, 409(6821), 695-697, doi:10.1038/35055518, 2001.
- 690 Janssen, N. A. H., Hoek, G., Simic-Lawson, M., Fischer, P., van Bree, L., Ten Brink, H., Keuken, M., Atkinson, R. W., Anderson, H. R., Brunekreef, B., and Cassee, F. R.: Black carbon as an additional indicator of the adverse health effects of airborne particles compared with PM10 and PM2.5, *Environ. Health Persp.*, 119, 1691-1699, doi:10.1289/ehp.1003369, 2011.
- Janssen, N. A. H., Gerlofs-Nijland, M. E., Lanki, T., Salonen, R. O., Cassee, F., Hoek, G., Fischer, P., 695 Brunekreef, B., and Krzyzanowski, M.: Health effects of black carbon, The WHO European Centre for Environment and Health, Bonn, Germany, World Health Organisation Regional Office for Europe, Copenhagen, Denmark, 2012.
- Keskinen J. and Rönkkö T.: Can real-world diesel exhaust particle size distribution be reproduced in the laboratory? A critical review, *Journal of the Air & Waste Management Association*, 60:10, 1245-1255, 700 doi:10.3155/1047-3289.60.10.1245, 2010.
- Kirchstetter, T. W., Novakov, T., and Hobbs, P. V.: Evidence that the spectral dependence of light absorption by aerosols is affected by organic carbon, *J. Geophys. Res.-Atmos.*, 109, D21208, doi:10.1029/2004JD004999, 2004.
- 705 Kondo, Y., Miyazaki, Y., Takegawa, N., Miyakawa, T., Weber, R. J., Jimenez, J. L., Zhang, Q., and Worsnop, D. R.: Oxygenated and water-soluble organic aerosols in Tokyo, *J. Geophys. Res.*, 112, D01203, doi:10.1029/2006JD007056, 2007.
- Laborde, M., Crippa, M., Tritscher, T., Jurányi, Z., Decarlo, P. F., Temime-Roussel, B., Marchand, N., Eckhardt, S., Stohl, A., Baltensperger, U., Prévôt, A. S. H., Weingartner, E., and Gysel, M.: Black carbon physical properties and mixing state in the European megacity Paris, *Atmos. Chem. Phys.*, 13, 5831-5856, 710 doi:10.5194/acp-13-5831-2013, 2013.
- Lack, D. A., Moosmüller, H., McMeeking, G. R., Chakrabarty, R. K., and Baumgardner, D.: Characterizing elemental, equivalent black, and refractory black carbon aerosol particles: a review of techniques, their limitations and uncertainties, *Anal. Bioanal. Chem.*, 406, 99-122, doi: 10.1007/s00216-013-7402-3, 2014.
- 715 Liu S., Aiken A. C., Gorkowski K., Dubey M. K., Cappa C. D., Williams L. R., Herndon S. C., Massoli P., Fortner E. C., Chhabra P. S., Brooks W. A., Onasch T. B., Jayne J. T., Worsnop D. R., China S., Sharma N., Mazzoleni C., Xu L., Ng N. L., Liu D., Allan J. L., Lee J. D., Fleming Z. L., Mohr C., Zotter P., Szidat S., and Prévôt A. S. H.: Enhanced light absorption by mixed source black and brown carbon particles in UK winter, *Nat. Commun.* 6:8435. doi: 10.1038/ncomms9435, 2015.
- 720 Moffet, R. C. and Prather, K. A.: In-situ measurements of the mixing state and optical properties of soot with implications for radiative forcing estimates, *Proc. Natl. Acad. Sci. USA*, 106, 11872-11877, doi:10.1073/pnas.0900040106, 2009.



- Moosmüller, H., Chakrabarty, R. K., and Arnott, W. P.: Aerosol light absorption and its measurement: a review, *J Quant. Spectrosc. RA*, 110(11), 844-878, doi:10.1016/j.jqsrt.2009.02.035, 2009.
- 725 Ng, N. L., Herndon, S. C., Trimborn, A., Canagaratna, M. R., Croteau, P. L., Onasch, T. B., Sueper, D., Worsnop, D. R., Zhang, Q., and Sun, Y. L.: An aerosol chemical speciation monitor (ACSM) for routine monitoring of the composition and mass concentrations of ambient aerosol, *Aerosol Sci. Tech.*, 45(7), 780–794, 2011.
- 730 Ning, Z., Chan, K. L., Wong, K. C., Westerdahl, D., Močnik, G., Zhou, J.H., and Cheung, C. S.: Black carbon mass size distributions of diesel exhaust and urban aerosols measured using differential mobility analyzer in tandem with Aethalometer, *Atmos. Environ.*, 80, 31-40, doi:10.1080/02786820500543324, 2013.
- Olstrup, H., Johansson, C., and Forsberg, B.: The use of carbonaceous particle exposure metrics in health impact calculations, *Int. J. Environ. Res. Public Health*, 13(3), doi:10.3390/ijerph13030249, 2016.
- 735 Pagels, J., Dutcher, D. D., Stolzenburg, M. R., McMurry, P. H., Gälli, M. E., and Gross, D. S.: Fine-particle emissions from solid biofuel combustion studied with single-particle mass spectrometry: Identification of markers for organics, soot, and ash components, *J. Geophys. Res. Atmos.*, 118, 859–870, doi:10.1029/2012JD018389, 2013.
- Park, S. S., Hansen, A. D. A., and Cho, Y.: Measurement of real time black carbon for investigating spot loading effects of Aethalometer data, *Atmos. Environ.*, 11, 1449–1455, doi:10.1016/j.atmosenv.2010.01.025, 2010.
- 740 Petit, J.-E., Favez, O., Sciare, J., Canonaco, F., Croteau, P., Močnik, G., Jayne, J., Worsnop, D., and Leoz-Garziandia, E.: Submicron aerosol source apportionment of wintertime pollution in Paris, France by double positive matrix factorization (PMF²) using an aerosol chemical speciation monitor (ACSM) and a multi-wavelength Aethalometer, *Atmos. Chem. Phys.*, 14, 13773-13787, doi:10.5194/acp-14-13773-2014, 2014.
- 745 Petit, J.-E., Favez, O., Sciare, J., Crenn, V., Sarda-Estève, R., Bonnaire, N., Močnik, G., Dupont, J.-C., Haefelin, M., and Leoz-Garziandia, E.: Two years of near real-time chemical composition of submicron aerosols in the region of Paris using an Aerosol Chemical Speciation Monitor (ACSM) and a multi-wavelength Aethalometer, *Atmos. Chem. Phys.*, 15, 2985–3005, doi:10.5194/acp-15-2985-2015, 2015.
- Polissar, A. V., Hopke, P. K., Paatero, P., Kaufmann, Y. J., Hall, D. K., Bodhaine, B. A., Dutton, E. G., and Harris, J. M.: The aerosol at Barrow, Alaska: long-term trends and source locations, *Atmospheric Environment*, 33(16), 2441–2458, doi:10.1016/S1352-2310(98)00423-3, 1999.
- 750 Poulain, L., Birmili, W., Canonaco, F., Crippa, M., Wu, Z. J., Nordmann, S., Spindler, G., Prévôt, A. S. H., Wiedensohler, A., and Herrmann, H.: Chemical mass balance of 300 °C non-volatile particles at the tropospheric research site Melpitz, Germany, *Atmos. Chem. Phys.*, 14, 10145-10162, doi:10.5194/acp-14-10145-2014, 2014.
- 755 Sandradewi, J., Prévôt, A. S. H., Szidat, S., Perron, N., Alfarra, M. R., Lanz, V. A., Weingartner, E., and Baltensperger, U.: Using aerosol light absorption measurements for the quantitative determination of wood burning and traffic emission contributions to particulate matter, *Environ. Sci. Technol.*, 42, 3316–3323, doi:10.1021/es702253m, 2008.
- Schmid, O., Artaxo, P., Arnott, W. P., Chand, D., Gatti, L. V., Frank, G. P., Hoffer, A., Schnaiter, M., and Andreae, M. O.: Spectral light absorption by ambient aerosols influenced by biomass burning in the Amazon



- 760 Basin, I.: Comparison and field calibration of absorption measurement techniques, *Atmos. Chem. Phys.*, 6, 3443-3462, doi:10.5194/acp-6-3443-2006, 2006.
- Schnaiter, M., Horvath, H., Mohler, O., Naumann, K. H., Saathoff, H., and Schock, O. W.: UV-VIS-NIR spectral optical properties of soot and soot-containing aerosols, *J. Aerosol Sci.*, 34, 1421–1444, doi:10.1016/S0021-8502(03)00361-6, 2003.
- 765 Segura, S., Estellés, V., Titos, G., Lyamani, H., Utrillas, M. P., Zotter, P., Prévôt, A. S. H., Mocnik, G., Alados-Arboledas, L., and Martínez-Lozano, J. A.: Determination and analysis of in situ spectral aerosol optical properties by a multi-instrumental approach, *Atmos. Meas. Tech.*, 7, 2373–2387, doi:10.5194/amt-7-2373-2014, 2014.
- Shindell, D., Kuylenstierna, J. C. I., Vignati, E., van Dingenen, R., Amann, M., Klimont, Z., Anenberg, S. C., 770 Muller, N., Janssens-Maenhout, G., Raes, F., Schwartz, J., Faluvegi, G., Pozzoli, L., Kupiainen, K., Höglund-Isaksson, L., Emberson, L., Streets, D., Ramanathan, V., Hicks, K., Oanh, N. T. K., Milly, G., Williams, M., Demkine, V., and Fowler, D.: Simultaneously mitigating near-term climate change and improving human health and food security. *Science*, 335, 183-189, doi:10.1126/science.1210026, 2012.
- Shiraiwa, M., Kondo, Y., Moteki, N., Takegawa, N., Sahu, L. K., Takami, A., Hatakeyama, S., Yonemura, S., 775 and Blake, D. R.: Radiative impact of mixing state of black carbon aerosol in Asian outflow, *J. Geophys. Res.*, 113(D24210), doi:10.1029/2008JD010546, 2008.
- Smith, K. R., Jerrett, M., Anderson, H. R., Burnett, R. T., Stone, V., Derwent, R., Atkinson, R. W., Cohen, A., Shonkoff, S. B., Krewski, D., Pope, C. A., Thun, M. J., and Thurston, G.: Public health benefits of strategies to reduce greenhouse-gas emissions: health implications of short-lived greenhouse pollutants, *Lancet*, 780 374(9707), 2091-2103, doi: 10.1016/S0140-6736(09)61716-5, 2009.
- Stein, A. F., Draxler, R. R., Rolph, G. D., Stunder, B. J. B., Cohen, M. D., and Ngan, F.: NOAA's HYSPLIT atmospheric transport and dispersion modeling system, *Bull. Am. Meteorol. Soc.*, 96(12), 2059–2077, doi:10.1175/BAMS-D-14-00110.1, 2015.
- Tian, J., Chow, J. C., Cao, J., Han, Y., Ni, H., Chen, L. W. A., Wang, X., Huang, R., Moosmüller, H., and 785 Watson, J. G.: A biomass combustion chamber: design, evaluation, and a case study of wheat straw combustion emission tests, *Aerosol Air Qual. Res.*, 15(5), 2104-2114, doi: 10.4209/aaqr.2015.03.0167, 2015.
- Virkkula, A., Mäkelä, T., Hillamo, R., Yli-Tuomi, T., Hirsikko, A., Hämeri, K., and Koponen, I. K.: A simple procedure for correcting loading effects of Aethalometer data, *J. Air Waste Manage.*, 57, 1214–1222, 790 doi:10.3155/1047-3289.57.10.1214, 2007.
- Virkkula, A., Chi, X., Ding, A., Shen, Y., Nie, W., Qi, X., Zheng, L., Huang, X., Xie, Y., Wang, J., Petäjä, T., and Kulmala, M.: On the interpretation of the loading correction of the Aethalometer, *Atmos. Meas. Tech.*, 8, 4415-4427, doi:10.5194/amt-8-4415-2015, 2015.
- Waked, A., Favez, O., Alleman, L. Y., Piot, C., Petit, J.-E., Delaunay, T., Verlinden, E., Golly, B., Besombes, J.-L., Jaffrezo, J.-L., and Leoz-Garziandia, E.: Source apportionment of PM₁₀ in a north-western Europe regional urban background site (Lens, France) using positive matrix factorization and including primary biogenic emissions, *Atmos. Chem. Phys.*, 14, 3325-3346, doi:10.5194/acp-14-3325-2014, 2014.



- Wei Y., Ma L., Cao T., Zhang Q., Wu J., Buseck P. R., and Thompson J. E.: Light scattering and extinction
800 measurements combined with laser-induced incandescence for the real-time determination of soot mass
absorption cross section, *Anal. Chem.*, 85(19), 9181–9188, DOI: 10.1021/ac401901b, 2013a.
- Wei Y., Zhang Q., and Thompson J. E.: Atmospheric black carbon can exhibit enhanced light absorption at high
relative humidity. *Atmos. Chem. Phys. Discuss.*, 13, 29413–29445, doi:10.5194/acpd-13-29413-2013,
2013b.
- Weingartner, E., Burtscher, H., and Baltensperger, U.: Hygroscopic properties of carbon and diesel soot
805 particles, *Atmos. Environ.*, 31(15), 2311–2327, doi:10.1016/S1352-2310(97)00023-X, 1997.
- Weingartner, E., Saathoff, H., Schnaiter, M., Streit, N., Bitnar, B., and Baltensperger, U.: Absorption of light by
soot particles: determination of the absorption coefficient by means of Aethalometers, *J. Aerosol Sci.*, 34,
1445–1463, doi:10.1016/S0021-8502(03)00359-8, 2003.
- Zhang, L., Sun, J. Y., Shen, X. J., Zhang, Y. M., Che, H., Ma, Q. L., Zhang, Y. W., Zhang, X. Y., and Ogren, J.
810 A.: Observations of relative humidity effects on aerosol light scattering in the Yangtze River Delta of China,
Atmos. Chem. Phys., 15, 8439–8454, doi:10.5194/acp-15-8439-2015, 2015.
- Zuberi, B., Johnson, K. S., Aleks, G. K., Molina, L. T., Molina, M. J., and Laskin, A.: Hydrophilic properties of
aged soot, *Geophys. Res. Lett.*, 32, L01807, doi:10.1029/2004GL021496, 2005.